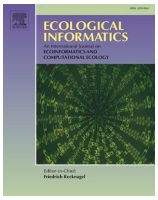
Ecological Informatics 100 (2026) 104130



Contents lists available at ScienceDirect

Ecological Informatics

journal homepage: www.elsevier.com/locate/ecolinf



Density-dependent emergence of collective phototaxis in a microcrustacean revealed by automated tracking

Elena Bellavere [a,*], Chang Liu [b,c], Gianluca Manduca [b,c], Giampaolo Rossetti [a], Donato Romano [b,c,*]

[a] Department of Chemistry, Life Sciences and Environmental Sustainability, University of Parma, Parco Area delle Scienze 11A, 43124 Parma, Italy
[b] The BioRobotics Institute, Sant'Anna School of Advanced Studies, Viale Rinaldo Piaggio 34, 56025, Pontedera, Pisa, Italy
[c] Department of Excellence in Robotics & A.I., Sant'Anna School of Advanced Studies, Pisa 56127, Italy

ARTICLE INFO

Keywords:
Heterocypris incongruens
Ostracoda
Phototaxis
Light-guided movement
Collective motion
Emergent coordination
Computer vision tracking

ABSTRACT

Light is a fundamental environmental cue influencing movement, habitat selection, and aggregation in aquatic organisms. While phototaxis has traditionally been studied at the level of individual responses, how social context and density modulate light-driven behavior in non-marine microcrustaceans remains poorly understood. Here, we investigated the phototactic response of the ostracod *Heterocypris incongruens* across three density regimes (single individuals, pairs, and groups of ≥30 individuals). We combined automated video tracking with quantitative behavioral analysis to extract spatial position, locomotor activity, and directional metrics across a light-off phase following a brief light pulse (<320 ms), a prolonged light stimulus, and a post-stimulus phase. This approach allowed us to resolve individual and emergent group-level dynamics within a unified analytical framework. Spatial attraction toward the light source and directional alignment were significantly enhanced in high-density groups, whereas isolated individuals and pairs did not exhibit comparable stimulus-dependent changes in spatial organization. Larger groups, but not isolated individuals, already oriented toward the brief onset pulse, suggesting that higher densities enhance responsiveness to transient directional cues. In contrast, locomotor variables such as velocity were largely independent of the light stimulus and reflected baseline differences between solitary and grouped conditions, indicating a decoupling between locomotor activity and directional control, with phototaxis expressed as a reorganization of movement direction rather than an increase in movement intensity. These findings suggest that the expression of light-guided movement is modulated by density-dependent effects, rather than being an individual-level trait.

1. Introduction

Light is a fundamental driver of ecological processes in aquatic environments, structuring habitats and influencing the behavior of organisms at multiple spatial and temporal scales. In both marine and inland waters, light conditions vary predictably with depth, turbidity, time of day, and season, generating heterogeneous environments in which organisms must continuously adjust their activity and position (Kirk, 2010; Shen et al., 2025). For many aquatic invertebrates, light is therefore not only a physical feature of the environment, but also a key source of ecological information, related to foraging opportunities, predator exposure, and habitat suitability (Kirk, 2010; Shen et al., 2025).

Phototaxis, defined as directed movement toward or away from a light source (Jékely, 2009), has been widely documented in many animal taxa, including crustaceans such as copepods, cladocerans, and amphipods (Forward Jr., 1980; Rajewicz et al., 2023; Stearns and Forward Jr., 1984). Experimental and field investigations have shown that phototactic responses in aquatic invertebrates can regulate vertical migration, aggregation patterns, and habitat selection, often in interaction with predation risk and physiological state (Bellot et al., 2022; Galbiati et al., 2023; Jensen et al., 1999; Michels and De Meester, 1998). Both positive and negative phototaxis have been reported, and the direction and magnitude of the response can vary depending on light intensity, spectral composition, and ecological context (Storz and Paul, 1998; Tao et al., 2019; Van Gool and Ringelberg, 2002). These

* Corresponding authors.
E-mail addresses: elena.bellavere@unipr.it (E. Bellavere), Chang.Liu@santannapisa.it (C. Liu), Gianluca.Manduca@santannapisa.it (G. Manduca), giampaolo.rossetti@unipr.it (G. Rossetti), Donato.Romano@santannapisa.it (D. Romano).

https://doi.org/10.1016/j.ecoinf.2026.104130
Received 15 June 2026; Received in revised form 6 September 2026; Accepted 5 October 2026
Available online 2 November 2026
1574-9541/© 2026 The Authors. Published by Elsevier B.V. This is an open access article under the CC BY license (http://creativecommons.org/licenses/by/4.0/).

findings suggest that phototaxis should not be regarded as a fixed species trait, but rather as a flexible behavioral response shaped by environmental circumstances.

While phototaxis is often analyzed at the level of isolated individuals (Dodson et al., 1997), many aquatic invertebrates naturally occur in groups, where interactions among conspecifics can influence movement decisions (Davidson et al., 2021; Jensen et al., 1999). Collective behavior, broadly defined as the emergence of coordinated patterns from local interactions among individuals, is increasingly recognized as a key component of ecological dynamics. Empirical studies across taxa have demonstrated that group size and density can modulate responsiveness to environmental cues, sometimes enhancing the detection of stimuli or amplifying directional responses (Berdahl et al., 2013; Suriyampola et al., 2022). A related but distinct possibility is that groups improve directional performance by combining variable individual estimates, as proposed by the "many-wrongs principle" (Codling et al., 2007; Simons, 2004). In aquatic invertebrates, aggregation can arise from simple behavioral rules yet lead to complex group-level outcomes such as clustering, alignment, or coordinated movement (Ambler, 2002; Burns et al., 2022; O'Brien, 1988; Ohtsuka et al., 1995). Understanding whether and how such collective effects influence phototaxis is essential for linking individual sensory responses to population-level patterns.

Among aquatic invertebrates, ostracods represent a useful model for investigating how responses to light are shaped by both environmental and social conditions. Ostracods are small bivalved crustaceans that are widespread in aquatic ecosystems, inhabiting marine, brackish, and freshwater environments across a wide range of ecological conditions (Horne et al., 2002). They play an important role in benthic and pelagic food webs, contributing to detrital processing and serving as prey for a variety of invertebrate and vertebrate predators. Their distribution and activity are shaped by multiple environmental factors, including substrate type, oxygen availability, and light conditions (Frenzel and Boomer, 2005; Zhang et al., 2024). In marine ostracods, particularly bioluminescent cypridinids, light has been shown to play a key role in behavioral organization, regulating the timing of courtship displays, when different species display, and how displays become synchronized in response to environmental and social cues (Gerrish and Morin, 2016; Hensley et al., 2023; Rivers and Morin, 2008). In some non-marine ostracods, light sensitivity and related behavioral changes have been observed, reflecting the ecological importance of light as a cue for both resource exploitation and predator avoidance (Bellavere et al., 2024). However, compared with marine systems, the role of light in shaping the behavior of non-marine ostracods remains much less explored, particularly in relation to social context.

In this context, an open question is whether the response to light in ostracods is primarily an intrinsic property of individuals or whether it emerges more strongly under group conditions. If social interactions contribute to the processing of environmental information, then increasing density may alter not only the magnitude but also the expression of the behavioral response. Investigating this possibility requires approaches that can simultaneously resolve individual or group-level movement and quantify directional behavior relative to a controlled stimulus.

Here, we address this question by quantifying the response of a non-marine ostracod species, *Heterocypris incongruens* (Ramdohr, 1808), to a localized light source across different group sizes under controlled laboratory conditions. This podocopid species is mainly benthic and can crawl on the sediment surface but can also perform short swimming bouts in the water column through the action of the well-developed natatory setae of the second antennae. It has also been shown to discriminate between different light stimuli and to exhibit associative learning (Bellavere et al., 2026; Romano et al., 2022). Using automated video tracking and quantitative behavioral metrics, we examine how proximity to light, locomotor activity, and directional orientation vary between isolated individuals and groups. By placing these measurements within an ecological and collective framework, this study aims to clarify the extent to which phototaxis in this non-marine ostracod reflects individual behavior versus an emergent property of group dynamics.

2. Materials and methods

2.1. Experimental setup and video recordings

Heterocypris incongruens is a cosmopolitan species inhabiting seasonal pools and small permanent water bodies (Meisch, 2000). The species is tolerant of highly eutrophic conditions and low oxygen content, including ponds heavily enriched by organic material from waterbirds (Meisch, 2000). Specimens were collected from a ditch at San Secondo Parmense (Parma, Italy; 44.9478° N, 10.2193° E) using hand nets during early spring 2024 (February–April). The population is parthenogenetic (Meisch, 2000). Adult females were identified and isolated under a stereomicroscope based on adult body size (1.2–1.9 mm) and selected for the experiments.

In the laboratory, *Heterocypris incongruens* was maintained in mineral water (specific electrical conductivity at 20 °C: 420 μS/cm) at room temperature under a natural photoperiod. Animals were fed fresh spinach leaves, which represent the preferred food source for this species under laboratory conditions (Miličić et al., 2015). One hour before each experiment, specimens were individually isolated and held in clean mineral water with physicochemical characteristics similar to those of the rearing water.

Each animal or group was tested only once. Individuals were transferred to a circular glass Petri dish (diameter: 100 mm, height: 10 mm) using a glass pipette. The dish was filled with a fixed volume of mineral water for each trial and thoroughly rinsed with mineral water between successive tests to avoid chemical carry-over between replicates.

The Petri dish was placed inside a white light box to provide a controlled environment. Ambient light was provided from above through a small aperture in the box lid, on which a daylight LED ring (approximately 200 lx, 6500 K) was mounted, just before the camera (Honor Lite; 108MP, 1080p), ensuring uniform illumination of the arena plane independent of laboratory lighting conditions.

Four warm-white LEDs (diameter: 10 mm; nominal forward voltage: 3.0–3.2 V; operating current: 18–20 mA) were mounted at the four cardinal positions of the arena rim, each at approximately 10 mm from the dish border. Each LED was angled approximately 60–80° downward relative to the arena's horizontal plane to maximize light diffusion into the dish side while minimizing specular reflections at the opposite border. For each trial, one LED was randomly selected as the active stimulus source. The active LED was connected in series with a 100 Ω resistor and controlled by an Arduino Uno microcontroller.

Three density treatments were used: single individuals ($n = 1$), pairs ($n = 2$), and large groups ($n \geq 30$, specifically 30 and 60 individuals).

Experiments were recorded on video and processed offline as described below. Each recording captured a single Petri dish observed from above at 25 frames per second (fps) under a fixed, top-down lighting geometry (see Fig. 1). Trials lasted approximately 55 s and were divided into three consecutive temporal phases: a post-pulse phase (light OFF, ~10 s) following a brief light pulse (< 320 ms) delivered at trial onset, a stimulus phase (light ON, ~30 s), and a post-stimulus phase (light OFF, ~10–15 s). The initial light pulse was delivered from the same direction as the subsequent sustained stimulus and while serving to synchronize the video protocol, was specifically utilized as a transient stimulus probe to assess whether group density influences directional responsiveness to brief environmental cues. Each trial contained one of three group conditions: 1 ostracod, 2 ostracods, or more than 30 ostracods (up to ~60).

The dataset analyzed here consisted of six independent replicates per group condition, each recorded under the same protocol and filmed in the same arena.

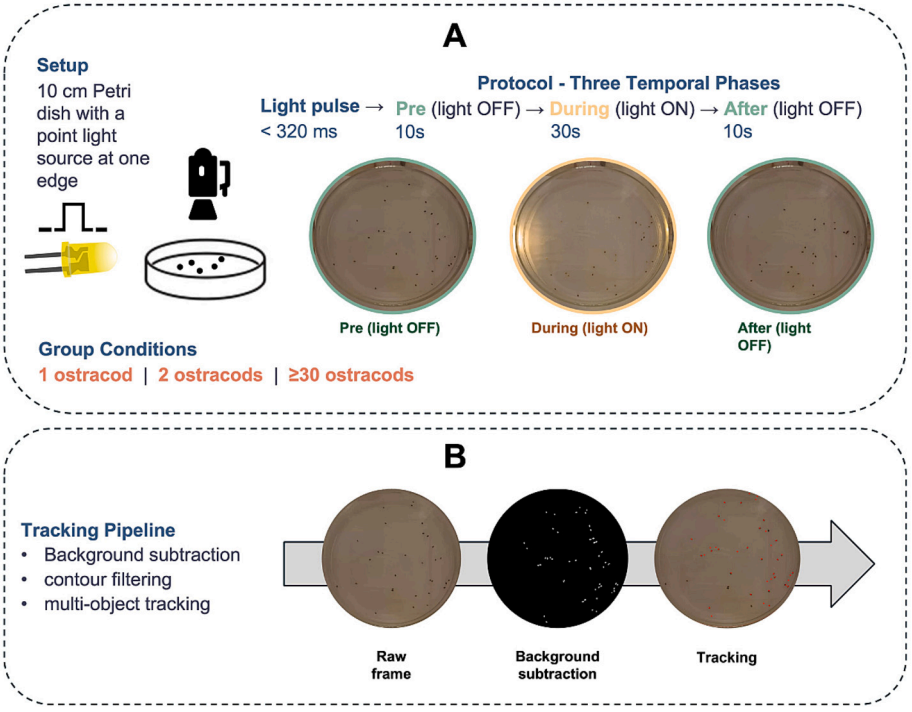


Fig. 1. Experimental setup and tracking pipeline: (A) Experimental setup consisting of 10 cm Petri dishes with a point light source positioned at one edge. Trials were conducted across three temporal phases: post-pulse (light OFF), during-light (light ON), and post-light (light OFF), and for different group sizes (1 ostracod, 2 ostracods, and ≥ 30 ostracods). (B) Image processing and tracking pipeline, including background subtraction, contour filtering, and multi-object tracking. Representative frames illustrate the raw input, background subtraction, and final tracking output.

2.2. Computer-vision pipeline

All behavioral data were obtained through a fully automated custom computer-vision pipeline developed by the authors and implemented in Python 3.12, based on OpenCV 4.12 for image processing, together with NumPy 2.2, SciPy 1.16, pandas 2.3 and matplotlib 3.10 for numerical analysis and visualization. The pipeline processed each frame independently and produced, for every frame, the spatial position of each ostracod and of each light source visible in the arena. The pipeline was organized into the following steps: (i) separation of the moving foreground (ostracods) from the static scene (arena, reflections, substrate), (ii) identification and validation of candidate objects in the foreground, and (iii) independent detection of the light source(s) on the raw frame. The steps are described below.

2.2.1. Arena segmentation

Since recordings occasionally contained marginal regions outside the Petri dish (bench surface, shadows, experimenter's hand), the usable region of each frame was restricted to the dish interior prior to any further processing. The circular arena was detected on the first frame using a Circular Hough Transform on a Gaussian-blurred grayscale image, searching for a single dominant circle whose radius ranged between 20% and 55% of the shorter image dimension. The detected circle (center $c = (c_x, c_y)$, radius r) defined an analysis mask that excluded all pixels outside the dish as well as a peripheral annulus of width 15 px adjacent to the rim. This rim exclusion removes the specular arc produced by the dish meniscus, which would otherwise be a strong source of false detections close to the boundary. The circle diameter also served as the basis for spatial calibration. With a real dish diameter of 100 mm and a measured diameter of approximately 1035 px, the conversion factor was $s \approx 0.0966$ mm/px, applied uniformly across all videos. All spatial metrics (distance, velocity) were converted to mm and mm/s accordingly.

2.2.2. Adaptive background modelling and foreground extraction

Because the animals moved continuously while the arena itself remained stationary, the video provided the information required to reconstruct the empty scene. A probabilistic background model was therefore built on-line using a Gaussian Mixture Model, in which the intensity history of each pixel is represented as a mixture of Gaussian components and continuously updated frame by frame. The mixture is maintained over a rolling history of 2000 frames, and the decision rule for foreground assignment is based on the squared Mahalanobis distance of the current pixel value from the Gaussian components describing the background:

$$(I(x, t) - \mu_k(x))^2 / \sigma_k^2(x) > \tau.$$

where I(x, t) is the intensity of pixel x at time t, μ_k and σ_k^2 are the mean and variance of the k-th Gaussian component of the background model at that pixel, and τ is a variance threshold set to 25. Pixels that do not fit any background component under this rule are labelled as foreground, producing a binary mask of moving objects. Two separate background models were maintained in parallel, one for the light-OFF phases and one for the light-ON phase: because the illumination step causes a sudden and global intensity shift, a single model would require a long re-adaptation transient during which detections are unreliable. Models were updated frame by frame with a learning rate $\alpha = 10^{-3}$, chosen to be fast enough to absorb slow illumination drift but slow enough that a single stationary ostracod would not be incorporated into the background within the time scale of a trial. Shadow detection was disabled, as the top-down illumination geometry used in the experiments does not produce cast shadows.

The raw foreground mask was then cleaned by morphological opening followed by closing, both performed with a 3×3 elliptical structuring element. Opening (erosion followed by dilation) removes isolated bright specks below the size of an ostracod, while closing (dilation followed by erosion) fills small holes inside the animal silhouettes and merges thin fractures caused by internal texture. This two-step operation ensured that each animal appeared as a single spatially

connected region rather than as a cluster of fragments.

2.2.3. Geometric and photometric validation

Connected components were extracted from the cleaned mask and treated as candidate animals. Because water meniscus reflections, dust particles, micro-bubbles, and illumination artifacts can produce foreground responses that pass the background subtraction step, every candidate was validated against a set of geometric and photometric criteria before being accepted as an ostracod. Specifically, a candidate with contour area A, perimeter P, convex-hull area A^H, and axis-aligned bounding-box dimensions (w, h) was retained only if all of the following conditions were satisfied:

- $5\ px^2 < A < 500\ px^2$, the biologically plausible silhouette range for a single ostracod at the recording scale;
- $0.2 < 4\pi A\ /\ P^2 < 1.2$, the isoperimetric (circularity) quotient, ensuring that highly irregular or fragmented contours are rejected;
- $A / A^H \geq 0.5$, the solidity, which penalizes concave or multi-lobed shapes typical of merged noise patches;
- $\max(w, h) / \min(w, h) \leq 4.0$, the aspect ratio, which rejects thin streak-like artifacts produced by rim reflections. The centroid of each accepted component was computed from the image moments as (μ_{10} / μ_{00}, μ_{01} / μ_{00}) and taken as the position of the corresponding animal in that frame. Two further photometric gates were then applied at the centroid level: (i) centroids lying within a 40 px radius from a detected light source were discarded, because this region is dominated by halo and glare artifacts, and (ii) centroids whose pixel intensity in the grayscale image exceeded 230 (on a 0–255 scale) were discarded as saturated reflections rather than animals.

A frame-level quality check was finally applied to reject entire frames when the detection output was implausible: frames in which more than 10% of the image area was classified as foreground (indicating a global illumination change, camera shake, or focus loss), frames in which the grayscale standard deviation fell below 5 (indicating a near-uniform, e.g. occluded, frame), and frames in which the number of validated candidates fell outside the plausible range [1,100] were flagged as invalid and excluded from downstream analysis.

2.2.4. Per-animal tracking and trajectory validation

To build continuous trajectories, validated detections were linked across consecutive frames by nearest-neighbor association with a maximum per-frame displacement of 15 px, a value well above the largest observed frame-to-frame displacement of an ostracod at 25 fps and well below the typical inter-animal distance. At each frame, every detection was associated with the closest active track within this radius; unmatched detections initiated new tracks, and tracks with no associated detection for more than 10 consecutive frames were terminated. For each track we maintained its age (number of frames since creation), the maximum Euclidean displacement from its initial position, and a counter of consecutive frames with per-frame displacement below a quiescence threshold $\varepsilon = 2$ px. Tracks younger than 5 frames, tracks whose maximum lifetime displacement never exceeded 3 px, and tracks that had remained quiescent for more than 120 frames (≈4.8 s at 25 fps) were excluded from the analysis as, respectively, transient noise, motionless artifacts, and sedimented debris being tracked as if alive.

2.2.5. Light-source detection

The position(s) of the light source(s) were detected independently on the raw frame, exploiting the fact that the stimulus produces a region of high image intensity along the arena rim. Pixels exceeding a brightness threshold were grouped into connected regions and subjected to the same geometric validation used for the animals, so that reflections or unrelated bright artifacts could be distinguished from the actual light sources. The brightness threshold was not fixed a priori but computed per video from the global frame intensity distribution, so that the detector automatically adapted to differences in camera exposure and stimulus intensity across recordings. When more than one bright region passed validation, typically a genuine light plus its specular image on the opposite side of the dish wall, all of them were retained as candidate light positions and treated equivalently in the subsequent analysis (see Section 2.3), since the behavioral question addressed here concerns the response to light as a directional cue rather than the preference for one specific source.

2.2.6. Quantitative validation of automated detection

To quantify the accuracy of the detection step independently of the downstream tracking and behavioral analysis, a stratified subset of frames was extracted from the 18 videos (six per density regime) and manually annotated by an expert observer. From each selected video, 21 frames were sampled uniformly across the three experimental phases (7 frames per phase: post-pulse, during-light and post-light), yielding 126 validated frames per density regime and 378 frames in total. On each frame, the annotator placed a point marker at the centroid of every ostracod visible in the arena using the VGG Image Annotator (VIA; Dutta and Zisserman, 2019), regardless of whether the animal was actively moving or motionless at that instant. The resulting ground-truth set was therefore completely independent of the automated pipeline output and intentionally more inclusive than the set of animals retained by the behavioral analysis, since the trajectory-level motion filters described in Section 2.2.4 (minimum lifetime displacement, quiescence threshold) deliberately exclude sedimented or motionless individuals from downstream metrics.

For each annotated frame, the manual and automated point sets were matched by greedy nearest-neighbor association under a fixed spatial tolerance of EPSILON_PX = 15 px (≈1.45 mm at the calibration of 1035 px = 100 mm, i.e. on the order of one ostracod body length). Each manual point was paired with the closest unmatched automated detection within this radius; pairs above the tolerance were not formed. Matched pairs were counted as true positives (TP), unmatched automated detections as false positives (FP), and unmatched manual points as false negatives (FN). From these counts we computed per-frame precision, recall and $F1 = 2 \cdot P \cdot R\ /\ (P + R)$, as well as the mean Euclidean localization error over matched pairs, reported both in pixels and in millimeters using the same calibration. Frame-level counts were aggregated by video, by experimental phase, and by density regime; aggregated precision, recall, F1 and mean localization error were computed from the pooled TP/FP/FN counts and pooled error distances rather than as averages of per-frame ratios, to give equal weight to each annotated animal. Because manual annotations include motionless ostracods that the pipeline deliberately filters out at the tracking stage, the resulting precision and recall represent a conservative lower bound on the performance of the pipeline as used in the behavioral analysis; localization accuracy, which is computed only on matched pairs, is unaffected by this scope mismatch and reflects the true centroid-extraction error.

2.3. Feature extraction

Three behavioral metrics were derived from the tracking output: (i) the minimum distance to the closest light source, (ii) the instantaneous velocity, and (iii) the relative heading angle with respect to the closest light. Metrics (i) and (iii) are directly related to the phototaxis hypothesis and are therefore computed relative to the light reference. Metric (ii) describes general locomotor behavior and is defined independently of light position.

2.3.1. Group summary position

Because many individuals were present in dense group condition (≥30 ostracods), and because consecutive per-frame positions of the same individual are strongly autocorrelated, we summarized the group at each frame by a single representative position. Specifically, at each frame t we computed the median of the x and y coordinates across all valid detections in the arena, resulting in a single ostracod position. The

median was preferred over the mean because it is robust to outlier detections (e.g., occasional stray ostracods or detection artifacts) and still tracks the central tendency of the group. All downstream metrics were computed from this time series of representative positions.

2.3.2. Minimum distance to the light source

At each frame t, the Euclidean distance from the median ostracod position P(t) to every detected light source was computed, and the minimum value, the distance to the closest light, was retained:

$$d_{min}(t) = \| P(t) - L \|$$

where L ranges over all light positions detected in that frame.

2.3.3. Instantaneous velocity

Velocity was computed as the magnitude of the frame-to-frame displacement of the median position, divided by the inter-frame interval Δt:

$$v(t) = \frac{\| P(t) - P(t-1) \|}{\Delta t}$$

Velocity is a feature of general locomotor activity and does not depend on light position.

2.3.4. Relative heading angle and cosine index

For each frame in which the median ostracod moved by at least 1 pixel (to avoid noise amplification when the group was quasi-stationary), two vectors were computed from the previous position P (t − 1):

The movement vector $m = P(t) - P(t-1)$, which gives the direction taken;

The light vector $l = L^* - P(t-1)$, where L^* is the closest light source at that frame.

Both vectors share the same origin $P(t-1)$, which is necessary to make their angular comparison meaningful. The relative angle between the two vectors was then defined as:

$$\alpha(t) = [\ atan2(my, mx) - atan2(ly, lx)\ ]\ mod\ 2\pi$$

so that $\alpha = 0^\circ$ corresponds to movement directly toward the closest light, $\alpha = 180^\circ$ to movement directly away from it, and $\alpha = 90^\circ$ / 270° to perpendicular movement. Since angles are circular, they cannot be treated with standard linear statistics. We therefore converted each angle to its cosine:

$$c(t) = cos(\alpha(t))$$

The cosine transform is a standard linearization. It takes values of +1 for motion toward the light, 0 for perpendicular motion (or random directions averaging out), and − 1 for motion away from the light.

2.3.5. Per-phase summary statistics

For each trial and each of the three phases (post-pulse, during-light, post-light), the frame-level metrics were aggregated into a single summary value per trial per phase, so that the statistical tests could be applied to one independent value per biological replicate. Summaries were chosen so that each metric retained a clear interpretation:

Minimum distance to light: mean of $d_{min}(t)$ over all frames of the phase. The temporal mean of an already light-referenced per-frame distance gives the average proximity of the (median) group to the light during that phase.

Velocity: mean of $v(t)$ over all frames of the phase, i.e. total distance / elapsed time.

Mean cosine of the relative angle: mean of c(t) over all valid frames of the phase. This quantity is bounded in [−1, +1] and is directly proportional to the projection of the mean movement vector onto the light direction.

Using summary statistics per trial, rather than raw per-frame values, is essential to satisfy the independence assumption of the statistical tests described below: if consecutive frames within a trial are highly autocorrelated then they cannot be treated as independent observations.

2.3.6. Spatial occupancy maps

Occupancy maps were computed from all validated detections, in order to describe how the ostracods distribute within the arena. Because the active LED was selected at random among the four rim positions, the coordinates of each trial were rotated about the arena center so that the light positions coincide across trials, and normalized by the dish radius. Detections from all videos of each density condition were then pooled, and their spatial density was estimated with a Gaussian kernel of approximately 3 mm (about two body lengths), with edge correction at the dish wall, normalized so that each map integrates to unity over the arena. Each map therefore gives the proportion of detections falling at each location, which makes the three density conditions comparable despite the large difference in the number of detections between them. The same detections were also used to follow over time the proportion of ostracods lying in the light zone, defined as the quarter of the arena closest to a light source, which corresponds to a radius of 26.6 mm around each source and sets the chance occupancy at 25% by construction; this proportion was averaged within one-second intervals for each trial and then across the trials of each condition.

2.3.7. Time spent close to the light and latency of the approach

Two further metrics were derived from the light-zone occupancy defined above, both referred to the light and both describing the temporal course of the response rather than its average magnitude. The time spent close to the light was computed, for each trial and each phase, as the proportion of individuals lying in the light zone averaged over all frames of that phase. As for the metrics above, this yields one value per trial per phase, so that the statistical tests are applied to one independent value per biological replicate. The latency of the approach was computed for the during-light phase only, as the time elapsed from light onset until this proportion first exceeded chance and remained above it for at least 2 s. Since the occupancy series is smoothed with a 1 s moving average, the required duration was set to twice this window, so that a crossing cannot be produced by the smoothing itself. Trials in which the criterion was never met within the stimulus were treated as censored rather than assigned a long latency.

2.4. Statistical analysis

All statistical analyses were carried out on the per-trial summary values described in the previous section. Because the behavioral measures considered here are not guaranteed to be normally distributed, and because the experimental design combines a repeated-measures structure (the three phases observed within each replicate) with an independent-groups structure (different replicates across group conditions), non-parametric rank-based tests were used throughout, as they make minimal distributional assumptions and are robust to outliers. Significance was assessed at the $\alpha = 0.05$ level, and p-values from post-hoc comparisons were adjusted for multiple testing using the Benjamini–Hochberg False Discovery Rate (BH-FDR) correction.

2.4.1. Within-group effect of phase

To test whether, for a given group size, the distribution of a given metric changed across the three temporal phases (post-pulse, during-light and post-light), we used the Friedman test. The Friedman test is the non-parametric analogue of a repeated-measures ANOVA: for each replicate (block), the three phase values are ranked, and the test statistic (Friedman χ^2) quantifies how consistently the phases are ranked across replicates. The test was run separately for each group condition (1, 2, and ≥ 30 ostracods) and for each metric.

When the Friedman test was significant, pairwise post-hoc comparisons were performed between phases (post-pulse vs during-light,

during-light vs post-light, post-pulse vs post-light) using the paired Wilcoxon signed-rank test, with BH-FDR correction across the three comparisons. Given the repeated-measures design, *p*-values of the Wilcoxon test were computed on the exact permutation distribution rather than on the large-sample normal approximation, which yields exact probabilities and avoids asymptotic biases.

2.4.2. Between-group effect of group size

To test whether, within a given phase, the metric differed across the three group conditions, we used the Kruskal–Wallis H test, the non-parametric analogue of a one-way ANOVA for independent samples. Replicates from different group conditions were treated as independent samples. The test was run separately for each phase (post-pulse, during-light and post-light) and for each metric.

When the Kruskal-Wallis test was significant, pairwise post-hoc comparisons between group conditions (1 vs 2, 1 vs ≥30, 2 vs ≥30) were performed using Dunn's test, with BH-FDR correction across the three comparisons.

2.4.3. Circular statistics of heading direction

Because heading angles are circular quantities, they cannot be averaged or compared using standard linear statistics. Two classical circular tests were therefore applied to the per-trial pooled angular data:

Rayleigh test: tests the null hypothesis that the angular sample is uniformly distributed on the circle (i.e., no preferred direction). A significant Rayleigh test indicates the presence of a mean direction, whichever direction that may be.

V-test (modified Rayleigh): tests the null hypothesis of uniformity against the alternative that the sample is concentrated around a specified direction. A significant V-test therefore provides direct evidence of orientation toward the light.

Both tests were applied to each combination of group condition (1, 2, ≥30 ostracods) and phase (post-pulse, during-light and post-light), pooling the angular data over replicates within that combination. In parallel, the mean cosine of the relative angle per trial was compared across phases and group conditions using the same Friedman + Wilcoxon and Kruskal-Wallis + Dunn's pipelines described above; this provides a between-trial, linear-statistics view of the same directional information that complements the pooled circular tests. Pooled per-frame angular statistics (Rayleigh test, V-test) are reported descriptively to assess overall directional tendency; statistical inference is based on per-trial mean cosines, treating each video as an independent unit.

2.4.4. Latency of the approach

Unlike the metrics above, the latency yields a single value per trial rather than one value per phase, so that only the between-group comparison applies to it. Moreover, in some trials the criterion was never met within the duration of the stimulus, thus the latency is a censored time-to-event variable, which cannot be treated with the rank tests described above without assigning an arbitrary value to those trials.

Latencies were compared across the three group conditions with the log-rank test, the standard non-parametric test for censored time-to-event data. It tests the null hypothesis that the latency distribution is the same in all group conditions, against the alternative that the approach occurs earlier in at least one of them. At each instant at which an event occurs, the test compares the number of events observed in each group with the number expected from its share of the trials still awaiting the event, and accumulates these differences over all event times. A significant log-rank test therefore indicates that the time taken to approach the light depends on group size. Trials in which the event never occurred remain among those awaiting it until the end of the stimulus, and therefore contribute to the expected counts without ever contributing an observed event. Pairwise comparisons between group conditions were performed with the same test and corrected with BH-FDR.

3. Results

3.1. Distance to light source

The analysis of the distance to the light source across experimental phases revealed a pattern consistent with a light-driven behavioral response in ostracods. Fig. 2 shows the resulting distance of the ostracods from the light source during the different phases (post-pulse, during-light, and post-light).

For trials involving a higher number of individuals (≥30 ostracods), the Friedman test indicated a significant effect of phase on distance ($\chi^2 = 6.33$, $p = 0.042$; Table 1), suggesting that group behavior changes in relation to light conditions. In contrast, no significant differences were observed for single individuals or pairs ($p > 0.05$), indicating that the effect emerges primarily at higher densities. Consistently, the Kruskal-Wallis test showed a significant difference among density groups specifically during the during-light phase ($H = 8.29$, $p = 0.016$; Table 1), while no significant differences were found in post-pulse or post-light conditions. Pairwise Wilcoxon post-hoc tests with BH-FDR correction did not reach significance in the ≥30 ostracods group, although the post-pulse vs during-light comparison showed a trend consistent with reduced distance to the light during the stimulus phase ($W = 0$, $p_adj = 0.094$). Dunn's post-hoc on the Kruskal-Wallis test indicated that the difference during-light is driven by the comparison between single ostracods and groups of ≥30 ostracods ($z = 2.87$, $p_adj = 0.012$). Together, these findings suggest that a light-driven reduction in distance to the stimulus emerges primarily at higher densities.

The spatial distribution underlying these differences is shown in Fig. 3. In the ≥30 ostracods regime, occupancy was broadly distributed over the arena during the post-pulse phase and became concentrated toward one end of the light axis during illumination. No comparable reorganization was observed for single individuals or pairs, whose occupancy remained scattered and showed no consistent relationship with the position of the light sources in any phase. The time course of this reorganization (Fig. 3B) further indicates that the aggregation did not form abruptly at stimulus onset but built up progressively over the illumination period, reaching its maximum toward the end of the stimulus and relaxing after light offset.

The time spent close to the light showed the same density-dependent pattern (Table 2, Fig. 4A). In the ≥30 ostracods condition the proportion of individuals in the light zone rose from 21.7% in the post-pulse phase to 35.2% during illumination, returning to 30.7% after light offset, a significant effect of phase (Friedman $\chi^2(2) = 8.33$, $p = 0.016$), whereas no effect was detected for single individuals ($\chi^2(2) = 2.55$, $p = 0.280$) or pairs ($\chi^2(2) = 1.00$, $p = 0.607$). Between conditions, the difference was significant only during illumination (Kruskal–Wallis $H(2) = 8.19$, $p = 0.017$), and Dunn's post-hoc indicated that it was driven by the ≥30 group, which differed from both single individuals ($p = 0.021$) and pairs ($p = 0.046$). Since the light zone covers a quarter of the arena, chance occupancy is 25%: groups of ≥30 ostracods were at chance level before the sustained stimulus and clearly above it during illumination, whereas single individuals remained below chance throughout. As in the analyses above, the pairwise Wilcoxon comparisons did not reach significance (all p_adj = 0.062), which reflects the resolution of the exact test with six replicates rather than the absence of an effect.

The latency of the approach differed markedly across conditions (Table 3, Fig. 4B). All six trials with ≥30 ostracods reached the criterion, with a median latency of 0.5 s, compared with five of six trials with pairs (median 7.8 s) and four of six with single individuals (median 12.6 s). The difference between conditions was significant (log-rank $\chi^2(2) = 8.53$, $p = 0.014$), and the pairwise comparisons identified the contrast between single individuals and groups of ≥30 ostracods ($p = 0.047$), with the comparison between pairs and groups of ≥30 ostracods showing a similar trend ($p = 0.098$). In two trials with ≥30 ostracods the criterion was already satisfied at light onset, indicating that

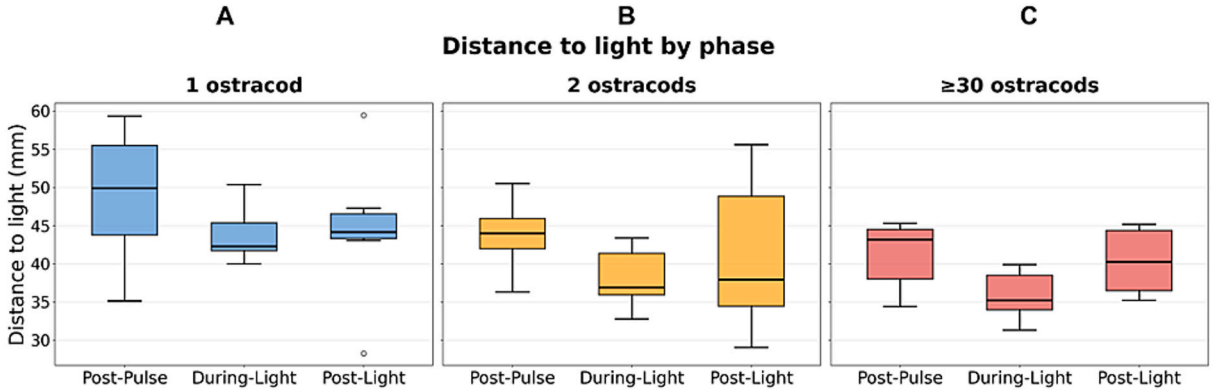


Fig. 2. Distance to the light source across experimental phases for different group sizes: (A) Single ostracod, (B) two ostracods, and (C) groups of ≥30 ostracods. Boxplots represent the distribution of distances measured during the post-pulse, during-light, and post-light phases.

Table 1
Friedman test (within-group, across phases) and Kruskal-Wallis test (between groups, within phase) on the minimum distance to the closest light source. Statistic refers to the Friedman χ^2 for within-group rows and the Kruskal-Wallis H for between-group rows.

Test	Group / Phase	Statistic	*p*-value	Significant
Friedman	1 ostracod	0.33	0.846	no
	2 ostracods	2.33	0.311	no
	≥30 ostracods	6.33	0.042	yes
Kruskal-Wallis	Post-pulse	2.67	0.264	no
	During light	8.29	0.016	yes
	Post light	0.89	0.641	no

these groups were already concentrated near the light following the initial pulse.

3.2. Velocity

The analysis of velocity revealed a baseline group-size effect on locomotor activity, largely independent of the light stimulus. Fig. 5 shows the velocity of the ostracods during the different phases (post-pulse, during-light and post-light).

The Friedman test showed a significant effect of phase only for single ostracods ($\chi^2 = 7.00$, $p = 0.030$; Table 4), while no effect was detected in the 2 ostracods ($\chi^2 = 3.00$, $p = 0.22$) or ≥ 30 ostracods ($\chi^2 = 0.00$, $p = 1.00$) groups. Pairwise Wilcoxon post-hoc tests with BH-FDR correction did not identify any significant pair of phases in any of the ostracod groups, although the post-pulse vs during-light and post-pulse vs post-light comparisons showed trends (both $p_adj = 0.094$). The Kruskal-Wallis test revealed a significant between-group effect in all three phases (post-pulse: $H = 13.66$, $p = 0.001$; during-light: $H = 10.71$, $p = 0.005$; post-light: $H = 9.91$, $p = 0.007$). Dunn's post-hoc with BH-FDR correction consistently identified the same pattern across phases: the 1 ostracod group differed significantly from both the 2 ostracods (all $p_adj \leq 0.046$) and the ≥30 ostracods (all $p_adj \leq 0.009$) groups, while the 2 vs ≥30 comparison was never significant (all $p_adj > 0.13$). This indicates that single ostracods move at a fundamentally different velocity from grouped ostracods regardless of the light phase, while grouped ostracods (2 and ≥ 30) do not differ from one another.

3.3. Directional orientation

Directional orientation toward the light was evaluated using the Rayleigh and V-tests on the pooled per-frame relative heading angles in each combination of group condition and phase (Table 5); these tests are reported descriptively, as statistical inference is based on the per-trial mean cosines (Table 6). In all group conditions, the during-light heading distributions departed significantly from uniformity and were concentrated toward the light (V-test: 1 ostracod, $V = 2.32$, $p = 0.010$; 2 ostracods, $V = 16.68$, $p < 0.001$; ≥30 ostracods, $V = 25.68$, $p < 0.001$). The strongest directional clustering was observed in the ≥30 ostracods group during the stimulus (Rayleigh $Z = 330.21$). However, Rayleigh's Z increases with sample size, thus it cannot be directly compared across group densities. A notable pattern emerged in the post-pulse phase of single ostracods: the Rayleigh test was significant ($Z = 3.96$, $p = 0.019$), indicating the presence of a preferred direction, but the V-test was not ($V = -0.41$, $p = 0.66$), meaning the preferred direction was not oriented toward the light. This highlights the complementary nature of the two tests and suggests that individual ostracods can exhibit a directional bias independent of the light stimulus.

Consistent with the circular tests above, the mean cosine of the relative angle provides a linear summary of how strongly the (median) group motion was directed toward the closest light at each trial (see Fig. 6). No significant phase effect was detected by the Friedman test in any of the group conditions (1 ostracod: $\chi^2(2) = 0.33$, $p = 0.85$; 2 ostracods: $\chi^2(2) = 2.33$, $p = 0.31$; ≥30 ostracods: $\chi^2(2) = 4.00$, $p = 0.14$; Table 6). This is consistent with the V-test results, which showed that orientation toward the light is already present to some extent in the post-pulse and post-light phases (with the exception of 1 ostracod in the post-pulse phase), so the average tendency of the motion toward the light does not necessarily change dramatically across phases when compared on a trial-by-trial basis.

In contrast, the Kruskal-Wallis test detected a significant between-group effect during the post-pulse ($H(2) = 7.52$, $p = 0.023$) and during-light ($H(2) = 6.19$, $p = 0.045$) phases, but not during the post-light phase ($H(2) = 3.79$, $p = 0.15$) (Table 6). The between-group difference observed in the post-pulse phase is consistent with differential detection of the onset pulse, where larger groups oriented toward the light source following the initial flick originating from the same direction as the subsequent sustained stimulus, whereas single individuals did not, suggesting that the transient stimulus may have been insufficient to produce a consistent directional response in isolated individuals. Notably, large groups already showed strong orientation toward the light during the post-pulse phase ($V = 15.76$), whereas single individuals exhibited only weak orientation even during sustained illumination ($V = 2.32$), further supporting the interpretation of a density-dependent effect on responsiveness to light cues (Table 5). Dunn's post-hoc with BH-FDR correction indicated that the main driver of this effect is the difference between 1 ostracod and ≥ 30 ostracods, which was significant in both the post-pulse phase ($z = -2.54$, $p = 0.033$) and the during-light phase ($z = -2.49$, $p = 0.039$). In addition, the 2 vs ≥30 ostracods comparison was significant in the post-pulse phase ($z = -2.16$, $p = 0.046$). The overall picture is that larger groups are more strongly oriented toward the light than individual ostracods, and this difference is already

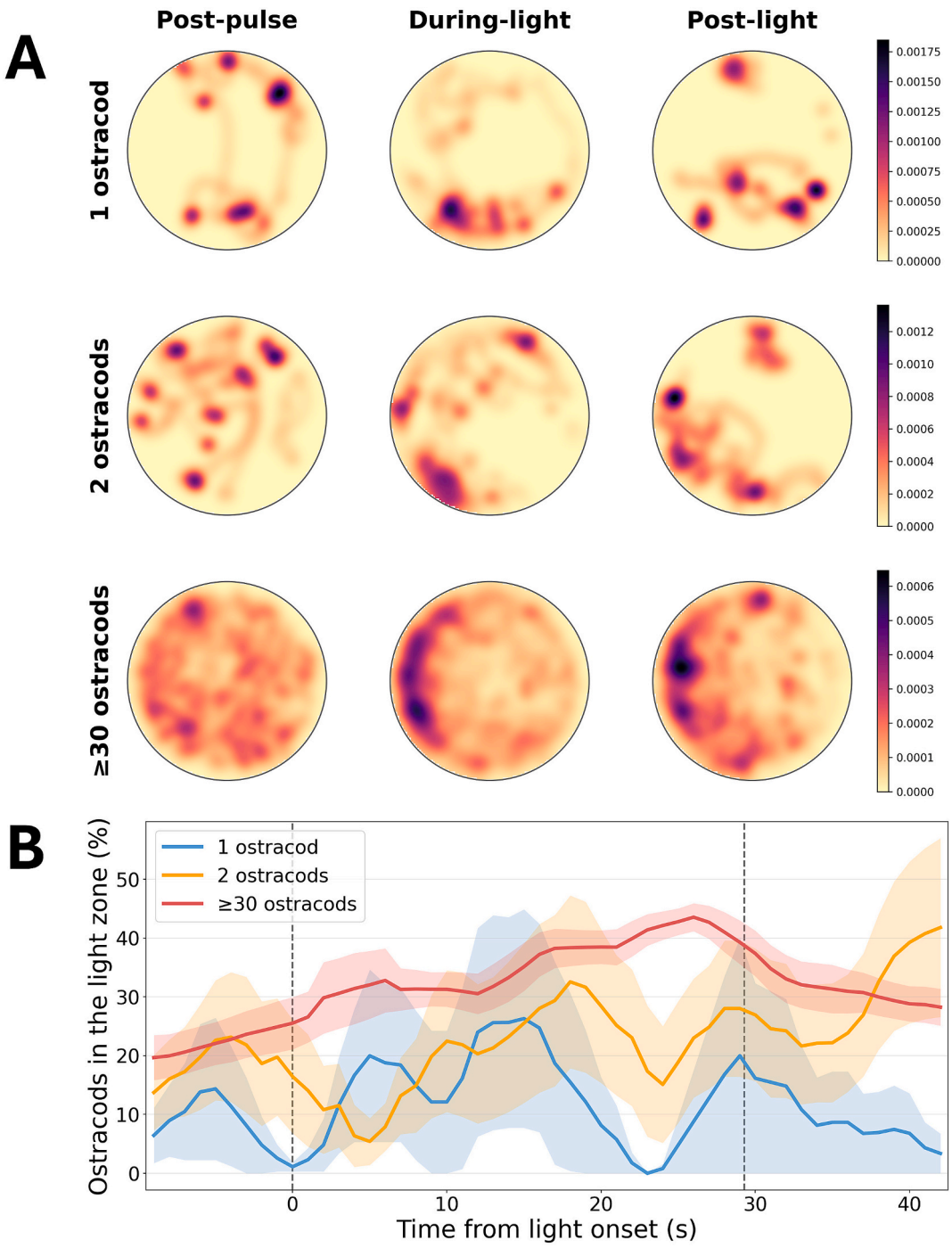


Fig. 3. (A) Spatial occupancy of the arena across density regimes and experimental phases. Occupancy maps for single individuals (top row), pairs (middle row) and groups of ≥30 ostracods (bottom row) during the post-pulse, during-light and post-light phases. Maps pool all validated detections from all videos of each regime; each arena was rotated so that the light positions match across panels. Color indicates the proportion of detections falling at each location, from light (unoccupied) to dark (crowded). Maps are normalized to unit total, so that regimes differing in the number of detections remain comparable; the color scale is set separately for each row. (B) Percentage of ostracods lying in the light zone, defined as the quarter of the arena closest to a light source, as a function of time, averaged across the videos of each condition and smoothed with a 5 s moving average to reduce the noise arising from the small number of individuals at low density. The shaded band around each line represents the standard error of the mean (SEM); dashed vertical lines mark the onset and offset of illumination and $t = 0$ is light onset.

measurable in the post-pulse phase, consistent with a group-level directional response to the onset pulse that was not seen in isolated individuals.

The markedly higher directional concentration during light in larger groups ($V = 25.68$) supports the interpretation that collective organization enhances the coherence of the phototactic response, and taken together with the velocity results, indicates that the phototactic response is primarily directional: ostracods change their heading toward light while their movement speed does not respond to the stimulus.

Notably, the weak directional bias shown by single individuals did not translate into a net accumulation near the source, where their occupancy of the illuminated region remained below chance in all phases (Fig. 3), indicating that an individual-level orientation bias is not by itself sufficient to produce spatial aggregation.

Table 2
Friedman test (within-group, across phases) and Kruskal–Wallis test (between groups, within phase) on the proportion of individuals in the light zone. Statistic refers to the Friedman χ^2 for within-group rows and the Kruskal–Wallis H for between-group rows.

Test	Group / Phase	Statistic	p-value	Significant
Friedman	1 ostracod	2.55	0.280	no
	2 ostracods	1.00	0.607	no
	≥30 ostracods	8.33	0.016	yes
Kruskal–Wallis	Post-pulse	3.80	0.150	no
	During light	8.19	0.017	yes
	Post light	3.76	0.153	no

Table 3
Latency of the approach to the light per group condition. The latency is the time elapsed from light onset until the proportion of individuals in the light zone first exceeded chance and remained above it for at least 2 s. Trials in which the criterion was never met within the stimulus are reported as censored. Statistic refers to the log-rank χ^2, with two degrees of freedom for the overall test and one for the pairwise comparisons, which were corrected with BH-FDR.

Group	Trials reaching criterion	Median latency (s)	Censored
1 ostracod	4 / 6	12.6	2
2 ostracods	5 / 6	7.8	1
≥30 ostracods	6 / 6	0.5	0

Test	**Groups compared**	**Statistic**	**p-value**	**Significant**
Log-rank	overall	8.53	0.014	yes
	1 vs 2 ostracods	0.99	0.320	no
	1 vs ≥30 ostracods	5.83	0.047	yes
	2 vs ≥30 ostracods	3.40	0.098	no

3.4. Validation of the automated detection pipeline

Across the 378 manually annotated frames, the automated detector recovered the great majority of ostracods present in the arena and localized them with sub-millimeter accuracy in all three density regimes (Table 7; Fig. 7). For single ostracods, 121 of 126 manual points were matched (recall = 0.96) at the cost of 45 false positives (precision = 0.73), giving F1 = 0.83 and a mean localization error of 3.28 px (0.32 mm). For pairs of ostracods, 212 of 252 manual points were matched (recall = 0.84, precision = 0.74, F1 = 0.79) with a mean localization error of 2.13 px (0.21 mm). For dense groups (≥30 ostracods), 3715 of 5040 manual points were matched (recall = 0.74, precision = 0.82, F1 = 0.78) with a mean localization error of 2.86 px (0.28 mm). Localization accuracy was therefore comparable across all three regimes and well below one ostracod body length (~1 mm), indicating that the centroids extracted by the detector are sufficiently precise to resolve individual animals for downstream behavioral analysis even at high density.

When disaggregated by experimental phase (Table 8), the post-light phase systematically produced the highest precision (0.95 for single ostracods, 0.97 for pairs, 0.92 for groups), confirming that the geometric and photometric gates of Section 2.2.3 effectively suppress halo and reflection artifacts once the illumination has stabilized. Recall was uniformly high in the single- and two-ostracod regimes (≥0.83 across all phases). In the dense-group regime, raw per-frame recall was lower (0.74); this figure is driven by two non-detection factors that do not

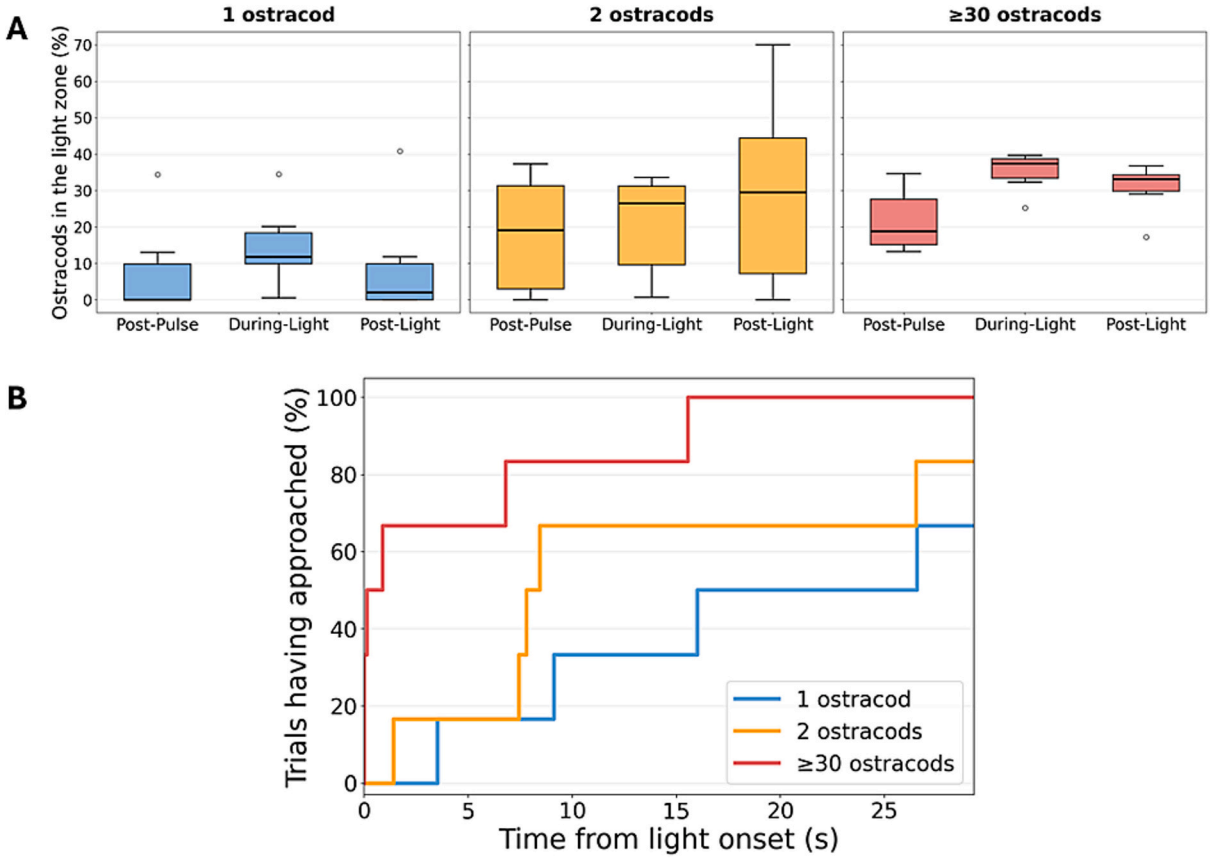


Fig. 4. Time spent close to the light and latency of the approach. (A) Proportion of ostracods lying in the light zone, the quarter of the arena closest to a light source, during the post-pulse, during-light and post-light phases, for 1, 2 and ≥ 30 ostracods. Each box summarizes the six trials of that condition, one value per trial. (B) Cumulative proportion of trials in which the group had approached the light, as a function of time from light onset. Each trial contributes a step at its latency; trials in which the criterion was never met do not contribute a step, so the curves plateau below 100% in the conditions where some replicates never approached.

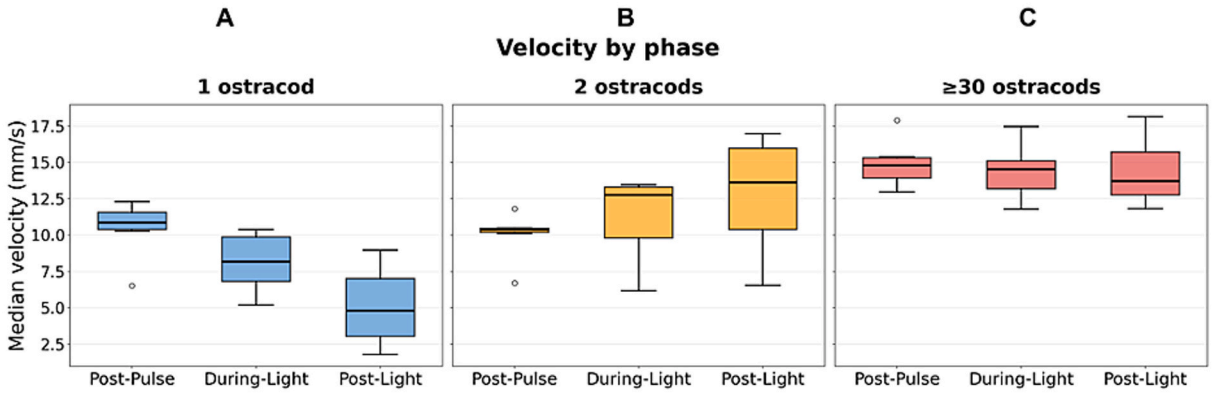


Fig. 5. Velocity across experimental phases for different group sizes. (A) Single ostracod, (B) two ostracods, and (C) groups of ≥30 ostracods. Boxplots represent the distribution of mean velocities (computed from the median ostracod trajectory) during the post-pulse, during-light, and post-light phases.

Table 4
Friedman test (within-group, across phases) and Kruskal-Wallis test (between groups, within phase) on the mean velocity. Statistic refers to the Friedman χ^2 for within-group rows and the Kruskal-Wallis H for between-group rows.

Test	Group / Phase	Statistic	p-value	Significant
Friedman	1 ostracod	7.00	0.030	yes
	2 ostracods	3.00	0.223	no
	≥30 ostracods	0.00	1.000	no
Kruskal-Wallis	Post-pulse	13.66	0.001	yes
	During light	10.71	0.005	yes
	Post light	9.91	0.007	yes

Table 6
Friedman test (within-group, across phases) and Kruskal–Wallis test (between groups, within phase) on the mean cosine of the relative heading angle. Statistic refers to the Friedman χ^2 for within-group rows and the Kruskal–Wallis H for between-group rows.

Test	Group / Phase	Statistic	p-value	Significant
Friedman	1 ostracod	0.33	0.846	no
	2 ostracods	2.33	0.311	no
	≥30 ostracods	4.00	0.135	no
Kruskal–Wallis	Post-pulse	7.52	0.023	yes
	During light	6.19	0.045	yes
	Post light	3.79	0.150	no

affect the behavioral analysis. First, manual annotations include motionless individuals that the pipeline deliberately excludes at the tracking stage (Section 2.2.4): a substantial fraction of the animals visible in any given frame of a dense-group recording are sedimented or transiently quiescent and are correctly filtered out by the minimum-displacement and quiescence gates before any behavioral metric is computed, so their absence from the detection output is a feature of the pipeline rather than a failure of it. Second, the first sampled frame of each phase systematically under-detected (e.g. 1 of 60 at frame 267 of VID_20250521_130324, 1 of 30 at frame 1011 of VID_20250521_140804), most likely reflecting the brief adaptation interval required by the background-subtraction model after a change in illumination; these per-phase warm-up frames account for a disproportionate share of the false negatives in the dense-group regime. Excluding the first sampled frame of each phase, per-frame recall in the dense-group regime exceeded 0.80 across all three experimental phases.

The precision and recall reported here therefore represent a conservative lower bound on the performance of the pipeline as used in Sections 3.1–3.3, while the sub-millimeter localization accuracy reflects the true centroid-extraction error. Taken together, these results demonstrate that the detection step of the pipeline localizes ostracod centroids with millimeter-scale accuracy across the full range of densities used in this study, that residual recall losses are concentrated in motionless individuals (which the pipeline correctly excludes from the behavioral analysis by design) and in per-phase background-subtraction warm-up frames at the boundary of each illumination phase, and that the centroid positions used in the subsequent analyses are quantitatively reliable.

4. Discussion

The present study demonstrates that phototactic behavior in *Heterocypris incongruens* is modulated by group size, revealing a density-dependent increase in directional coherence toward localized light stimuli. Beyond the specific case of ostracod phototaxis, these results provide an empirical example of how collective directional organization can emerge from variable individual responses when individuals interact at sufficient densities. The controlled laboratory conditions used here, although simplified compared with natural temporary pools, allowed the isolation of the effects of light and group size from other ecological factors such as predation, interspecific interactions, and

Table 5
Rayleigh and V-tests on the pooled per-frame relative heading angles per group condition and phase. The Rayleigh test assesses departure from uniformity (presence of any preferred direction), while the V-test assesses concentration toward 0° (i.e., toward the closest light source). The "Toward light" column indicates whether the V-test is significant.

Group	Phase	Rayleigh Z	Rayleigh p	V	V p	Toward light
1 ostracod	Post-pulse	3.96	0.019	−0.41	0.660	no
1 ostracod	During light	3.32	0.036	2.32	0.010	yes
1 ostracod	Post light	5.16	0.006	1.67	0.048	yes
2 ostracods	Post-pulse	4.68	0.009	2.47	0.007	yes
2 ostracods	During light	167.66	<0.001	16.68	<0.001	yes
2 ostracods	Post light	30.00	<0.001	7.74	<0.001	yes
≥30 ostracods	Post-pulse	133.70	<0.001	15.76	<0.001	yes
≥30 ostracods	During light	330.21	<0.001	25.68	<0.001	yes
≥30 ostracods	Post light	83.57	<0.001	12.67	<0.001	yes

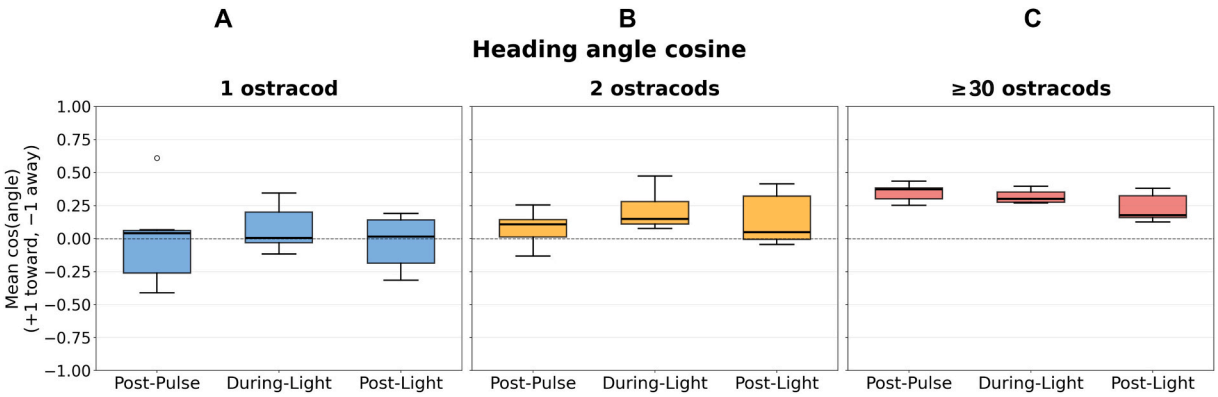


Fig. 6. Directional alignment toward the light source across experimental phases for different group sizes. (A) Single ostracod, (B) two ostracods, and (C) groups of ≥30 ostracods. Boxplots represent the distribution of the mean cosine of the relative angle, indicating the degree of alignment of movement toward the light source during the post-pulse, during-light, and post-light phases. Higher values indicate stronger directional alignment toward the light.

Table 7
Aggregate detection-validation metrics by density regime. $n = 126$ frames per regime (21 frames per video × 6 videos). Manual pts.: total manually annotated points. Auto dets: total automated detections. TP/FP/FN: matched pairs, unmatched auto detections, unmatched manual points. Localization error (Loc. err.) is computed over matched pairs only, in pixels and millimeters.

Density regime	Frames	Manual pts	Auto dets	TP	FP	FN	Precision	Recall	F1	Loc. err. (px)	Loc. err. (mm)
1 ostracod	126	126	166	121	45	5	0.729	0.960	0.829	3.28	0.317
2 ostracods	126	252	287	212	75	40	0.739	0.841	0.787	2.13	0.205
≥30 ostracods	126	5040	4514	3715	799	1325	0.823	0.737	0.778	2.86	0.277

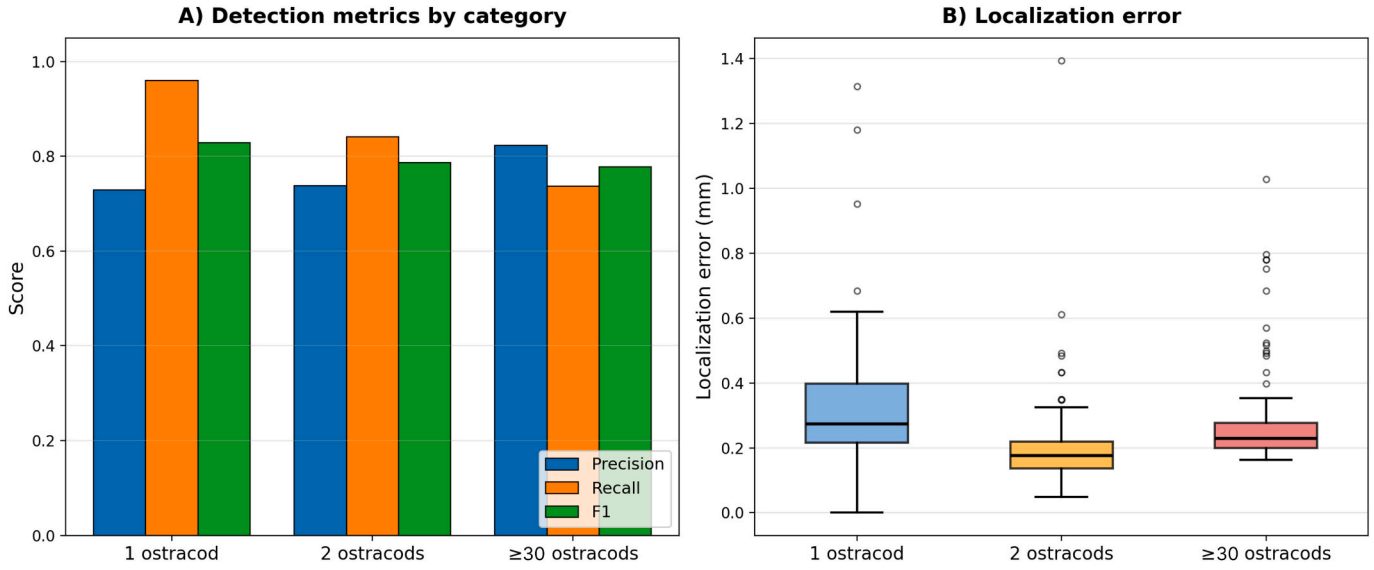


Fig. 7. Quantitative validation of the automated detection pipeline against manual point annotations ($n = 126$ frames per density regime; 378 frames in total). (A) Per-frame precision, recall and F1 for the three density regimes (1 ostracod, 2 ostracods, and ≥ 30 ostracods), aggregated from pooled TP, FP and FN counts. (B) Distribution of Euclidean localization error over matched manual–automatic pairs, in millimeters, for each density regime. The dashed horizontal line marks 1 mm, corresponding to approximately one ostracod body length; the median localization error is below this reference in all three regimes.

habitat heterogeneity.

In parallel, this study highlights the role of automated computer-vision tracking as a quantitative tool for resolving collective behavioral dynamics in small aquatic invertebrates. The pipeline enabled continuous extraction of spatial trajectories and directional metrics across temporal phases of stimulation, providing a framework to link individual motion to emergent group-level patterns. Such approaches are increasingly used to study collective motion as a system-level phenomenon arising from local interactions rather than independent individual responses (Bechinger et al., 2016; Berman, 2018; Calovi et al., 2018; Dell et al., 2014).

This result is particularly relevant given the locomotor ecology of *H. incongruens*. Unlike many aquatic invertebrates that exploit the water column in three dimensions, this species exhibits a predominantly two-dimensional, benthic-associated locomotor pattern typical of non-marine ostracods (Danielopol and Swanson, 2019). It inhabits shallow temporary and permanent water bodies characterized by fine sediments and limited structural complexity (Meisch, 2000). Under these conditions, spatial proximity and local interactions among individuals may play a stronger role in shaping mesoscale organization.

Table 8
Detection-validation metrics broken down by experimental phase (post-pulse, during-light, post-light) within each density regime. $n = 42$ frames per cell (7 frames per phase × 6 videos). Aggregated precision, recall and F1 are computed from pooled TP/FP/FN counts; mean localization error (Loc. err.) is averaged over matched pairs in millimeters.

Density regime	Phase	Frames	TP	FP	FN	Precision	Recall	F1	Loc. err. (mm)
1 ostracod	post-pulse	42	38	22	4	0.633	0.905	0.745	0.308
1 ostracod	during-light	42	41	21	1	0.661	0.976	0.788	0.321
1 ostracod	post-light	42	42	2	0	0.955	1.000	0.977	0.321
2 ostracods	post-pulse	42	71	25	13	0.740	0.845	0.789	0.217
2 ostracods	during-light	42	70	48	14	0.593	0.833	0.693	0.214
2 ostracods	post-light	42	71	2	13	0.973	0.845	0.904	0.187
≥30 ostracods	post-pulse	42	1245	445	435	0.737	0.741	0.739	0.285
≥30 ostracods	during-light	42	1235	249	445	0.832	0.735	0.781	0.269
≥30 ostracods	post-light	42	1235	105	445	0.922	0.735	0.818	0.276

While directional orientation toward the light was observed across all densities, coherence increased markedly in larger groups. In these conditions, the response was primarily directional rather than kinematic, with the group median trajectory shifting toward the light while locomotor speed remained largely unaffected. Isolated individuals showed lower apparent velocities than grouped animals, independently of light conditions. Larger groups, by contrast, showed reduced speed variability. Moreover, isolated individuals and pairs did not show a clear reduction in distance from the light source. Aggregation became evident only at higher density, when light-mediated orientation was apparently reinforced by group context and translated into a coherent spatial response. The spatial distribution of the ≥30 individual groups shifted from broadly distributed across the arena in the post-pulse phase to concentrated toward the light axis during illumination. In contrast, no comparable reorganization was observed for isolated individuals or pairs, whose occupancy remained scattered and showed no significant relationship with light position. Light-zone occupancy for isolated individuals remained below the chance level across all phases despite the weak, general directional bias, indicating that a noisy individual-level orientation alone is insufficient to produce spatial proximity to the stimulus. In groups, the above-chance occupancy of the light zone was reached, on average, shortly after the onset of the sustained stimulus, a latency significantly shorter than in isolated individuals. Importantly, collective performance relies on both directional accuracy and decision speed, as faster responses by groups can provide a significant advantage (Biro et al., 2016; Sumpter and Pratt, 2009). Part of this difference reflects the use of a median-based group trajectory, which reduces the effect of opposing individual displacements in dense groups. Accordingly, group-level trajectories should be interpreted as descriptors of emergent spatial organization rather than direct analogs of individual motion. However, because density effects primarily involved directional coherence and spatial aggregation rather than speed modulation, the observed pattern is not readily attributable to the median-based trajectory alone. Similar reductions in locomotor variability between isolated and grouped animals have been observed in other collective systems, including schooling fish (Herbert-Read et al., 2013; Klamser et al., 2021), suggesting that local interactions can stabilize directional order.

Larger groups exhibited directional orientation toward the light already during the post-pulse phase, the period immediately following the brief light pulse originating from the same direction as the later sustained stimulus. This suggests that collective organization may amplify weak or transient environmental cues and reduce the influence of variable individual directional responses, potentially allowing groups to extract directional information that is insufficient to drive consistent responses at the individual level. Thus, the presented findings seem more consistent with a reduction in individual-level variability through group-level pooling of directional responses than with density-dependent modulation of stimulus detection, in which individuals lack reliable directional information, and a response emerges only at the collective level (e.g., Berdahl et al., 2013).

The observation that group orientation to the stimulus is enhanced compared with that of isolated individuals is consistent with the "many-wrongs principle" (Bergman and Donner, 1964; Codling et al., 2007; Hamilton, 1967; Simons, 2004; Wallraff, 1978). Under the latter framework, individual organisms act as noisy information-processing units whose variable responses may be combined at the group level. In this context, collective interactions could allow the averaging of individual-level variability consistent with directional and spatial performance exceeding that of isolated individuals. However, the present study did not directly test whether the ostracods pooled directional information. Nevertheless, the "many-wrongs principle" provides a useful framework for interpreting the observed density-dependent behavior of *H. incongruens*.

Such dynamics align with theoretical and empirical work demonstrating that collective behavior can emerge from simple local interaction rules without centralized coordination or complex cognition and sociality (De and Chakraborty, 2022; Durieux et al., 2014; Jeanson et al., 2012; Robert et al., 2013). Leaderless local interactions, such as simple alignment, local neighboring copying, or weighted averaging based on individual behavioral traits, can generate coordinated movement and may improve collective navigation, although the degree of improvement partly depends on the individual-level tradeoff between environmental and interaction cues (Codling and Bode, 2014; Mann et al., 2024; Sasaki et al., 2022). According to this interpretation, rather than reflecting centralized coordination, the pattern observed is consistent with density-dependent self-organization, in which weak individual biases are amplified through short-range interactions (Bastien and Romanczuk, 2020; Cavagna and Giardina, 2014; Couzin et al., 2002; Vicsek and Zafeiris, 2012).

Navigational performance under the "many-wrongs principle" can improve nonlinearly with group size up to an optimal threshold, beyond which crowding-related effects such as collision avoidance can impair directional efficiency (Codling et al., 2007; Codling and Bode, 2014). In this study, groups of 30 or more individuals showed the strongest collective response among the densities tested. This pattern is compatible with a density-dependent reduction in the influence of individual-level variability, although the present study did not establish a specific group-size threshold or demonstrate that error suppression was the underlying mechanism. More broadly, the "many-wrongs principle" has been proposed to operate across biological scales and has been observed across taxa (e.g., Codling et al., 2007; Sasaki et al., 2022; Simons, 2004), as well as in non-animal systems such as cellular migration (Colizzi et al., 2020). The present findings suggest that *H. incongruens*, a small aquatic invertebrate with a comparatively simple nervous system, may fit within this broader pattern.

Previous studies have described ostracod aggregation as a by-product of environmental constraints in temporary habitats (Allee, 1931; Klie, 1926; Nuttall and Fernando, 1970). In *Heterocypris incongruens*, laboratory observations similarly reported aggregations interpreted as independent movement leading to incidental clustering (Kesling, 1951; Nuttall and Fernando, 1970). Field observations of

collective movement in temporary ponds were likewise interpreted as individual responses to environmental fluctuations (Benzie, 1984). The present results extend these interpretations by suggesting that apparent aggregation and directional coherence may arise from density-dependent amplification of weak individual responses. Reports of group-associated predatory behavior in this species (Nuttall and Fernando, 1970; Ottonello and Romano, 2011; Rossi et al., 2011; Sohn and Kornicker, 1972) further indicate that local interactions can generate context-dependent collective effects.

Responses to local cues may be particularly relevant in podocopid ostracods, which rely strongly on non-visual sensory modalities (Bellavere et al., 2024). Chemical and mechanosensory cues can modulate aggregation and locomotor activity in *Heterocypris incongruens* (Miličić et al., 2019). Although pheromonal communication is unlikely in obligate parthenogenetic populations, mechanosensory and indirect environmental cues may still contribute to density-dependent spatial organization (Wiese, 1996; Yu et al., 2024).

More broadly, environmental and endogenous cues such as light, diel cycles, and rhythmicity are known to structure spatial organization in aquatic invertebrates (Cottier et al., 2006; Enright and Hamner, 1967; Graham et al., 2001; Kao et al., 2010; Ringelberg, 1995). Density-dependent collective responses have been widely reported in crustaceans with relatively simple nervous systems (Clutter, 1969; Macquart-Moulin, 1973; Modlin, 1990; Pijanowska and Kowalczewski, 1997; Wiese, 1996). In relation to light, microcrustaceans such as Daphnia exhibit phototactic attraction and density-dependent vortex formation, where coherent swarming emerges only at high densities (Gerhardt et al., 2006; Jensen et al., 1998; Ordemann et al., 2003; Rajewicz et al., 2023). Similarly, copepods form light-dependent aggregations that vary with diel and environmental conditions (Buskey et al., 1995; Flierl and Woods, 2015; Leising and Yen, 1997; Okubo, 1980).

From an ecological perspective, density-dependent aggregation may enhance microhabitat selection, predator avoidance, or resource exploitation, although its adaptive value is likely context-dependent (Bukovinszky et al., 2013; Jensen and Larsson, 2002). In temporary pools, such mechanisms could facilitate aggregation in favorable microhabitats while maintaining behavioral flexibility across environmental gradients.

Unraveling the mechanisms underlying this phenomenon will require experiments explicitly separating physical interactions, chemical and mechanosensory cues, and fine-scale movement rules such as changes in turning behavior or residence time near light sources. More generally, these results show that population-level environmental responsiveness can emerge from density-dependent interactions even in organisms with relatively simple sensory systems, highlighting the limited predictive power of individual-level phototactic thresholds for collective behavior.

5. Conclusions

This study investigated how the non-marine ostracod *Heterocypris incongruens* responds to a localized light stimulus under different density conditions, using automated video tracking to quantify spatial position, locomotor activity, and directional orientation across post-pulse, during-light and post-light phases. The computer-vision pipeline enabled a high-resolution, quantitative description of both individual and collective movement, allowing phototactic responses to be evaluated within a unified spatial and temporal framework.

The results show that the effect of light on spatial behavior is strongly density dependent. A reduction in distance to the light source and a coherent directional alignment toward the stimulus were observed primarily in high-density conditions ($\geq$30 individuals), whereas isolated individuals and pairs did not exhibit comparable changes in spatial organization. These findings indicate that directional phototactic responses become progressively more coherent with increasing group size, suggesting a transition in the expression of the behavior across density regimes. Additionally, larger groups were already oriented toward a brief onset pulse originating from the same direction as the subsequent sustained stimulus, whereas this pulse failed to drive directional orientation in isolated individuals. This observation suggests that the group-level response may arise from density-dependent amplification of weak or transient directional cues.

In contrast, locomotor variables such as velocity were largely independent of the light stimulus and instead reflected consistent differences between isolated and grouped animals. This pattern indicates that the primary effect of the stimulus is on directional organization rather than on overall activity levels and supports the interpretation of phototaxis as a reorganization of movement direction rather than a global modulation of locomotor output.

Overall, these results suggest that phototaxis in *H. incongruens* is not solely an individual-level response to light but depends on group context, which shapes both the directional and spatial organization of the response. Light-guided movement therefore emerges more clearly in group contexts, highlighting the importance of considering collective dynamics when interpreting sensory-driven behavior in aquatic microinvertebrates. Future work should extend this framework to a broader range of densities, stimulus regimes, and species, and incorporate explicit measurements of local interaction rules to disentangle the mechanisms underlying density-dependent amplification of directional responses.

CRediT authorship contribution statement

Elena Bellavere: Writing – review & editing, Writing – original draft, Methodology, Investigation, Data curation, Conceptualization. **Chang Liu:** Writing – review & editing, Validation, Software, Formal analysis. **Gianluca Manduca:** Writing – review & editing, Validation, Software, Formal analysis. **Giampaolo Rossetti:** Writing – review & editing, Writing – original draft, Supervision. **Donato Romano:** Writing – review & editing, Writing – original draft, Supervision, Methodology, Conceptualization.

Declaration of competing interest

The authors declare that they have no known competing financial interests or personal relationships that could have appeared to influence the work reported in this paper.

Acknowledgments

This scientific research was supported by the HORIZON-EIC-2023-PATHFINDEROPEN-01, SENSORBEES “Sensorbees are ENhanced Self-ORganizing Bio-hybrids for Ecological and Environmental Surveillance” (Grant agreement ID: 101130325), the HORIZON-CL6-2024-BIODIV-01 BioDiMoBot “Autonomous Longtime Aquatic Biodiversity and Ecology Monitoring Robot” (Grant agreement ID: 101181363) and the Project funded under the National Recovery and Resilience Plan (NRRP), Mission 4 Component 2 Investment 3.1 - Fund for the implementation of an integrated system of research and innovation infrastructures – of Italian Ministry of University and Research funded by the European Union - NextGenerationEU; Project identification code IR0000036, Concession Decree No. 3262 of 28/12/2021 adopted by the Italian Ministry of University and Research, CUP J13C22000400007, “Biorobotics Research and Innovation Engineering Facilities” (BRIEF).

Data availability

The dataset containing the original videos, the post-processed videos, and each step of the pipeline validation is publicly available in the Zenodo repository at https://doi.org/10.5281/zenodo.20465029.

References

Allee, W.C., 1931. Animal aggregations: a study in general sociology. University of Chicago Press. https://doi.org/10.5962/bhl.title.7313.

Ambler, J.W., 2002. Zooplankton swarms: characteristics, proximal cues and proposed advantages. Hydrobiologia 480, 155–164. https://doi.org/10.1023/A:1021201605329.

Bastien, R., Romanczuk, P., 2020. A model of collective behavior based purely on vision. Sci. Adv. 6 (6), eaay0792. https://doi.org/10.1126/sciadv.aay0792.

Bechinger, C., Di Leonardo, R., Löwen, H., Reichhardt, C., Volpe, G., Volpe, G., 2016. Active particles in complex and crowded environments. Rev. Mod. Phys. 88 (4), 045006. https://doi.org/10.1103/RevModPhys.88.045006.

Bellavere, E., Matzke-Karasz, R., Romano, D., Rossetti, G., 2024. Structure and functional implications of photoreceptive systems in non-marine ostracods: a review. Hydrobiologia 851, 4051–4075. https://doi.org/10.1007/s10750-024-05587-2.

Bellavere, E., Mesquita-Joanes, F., Romano, D., Rossetti, G., 2026. Evidence of visual learning and wavelength differential responses in three podocopids (Crustacea: Ostracoda). BMC Biol. 24, 164. https://doi.org/10.1186/s12915-026-02640-5.

Bellot, M., Gómez-Canela, C., Barata, C., 2022. Phototactic behaviour and neurotransmitter profiles in two *Daphnia magna* clones: vertical and horizontal responses to fish kairomones and psychotropic drugs. Sci. Total Environ. 830, 154684. https://doi.org/10.1016/j.scitotenv.2022.154684.

Benzie, J.A.H., 1984. Small scale diurnal migrations by *Heterocypris incongruens* (Ramdohr, 1808) (Ostracoda: Cyprididae) in a temporary Pool, Ghana, West Africa. J. Crustac. Biol. 4 (1), 63–65. https://doi.org/10.2307/1547896.

Berdahl, A., Torney, C.J., Ioannou, C.C., Faria, J.J., Couzin, I.D., 2013. Emergent sensing of complex environments by mobile animal groups. Science 339 (6119), 574–576. https://doi.org/10.1126/science.1225883.

Bergman, G., Donner, K.O., 1964. An analysis of the spring migration of the common scoter and the long-tailed duck in southern Finland. Acta Zool. Fenn. 105, 1–59.

Berman, G.J., 2018. Measuring behavior across scales. BMC Biol. 16 (1), 23. https://doi.org/10.1186/s12915-018-0494-7.

Biro, D., Sasaki, T., Portugal, S.J., 2016. Bringing a time–depth perspective to collective animal behaviour. Trends Ecol. Evol. 31 (7), 550–562. https://doi.org/10.1016/j.tree.2016.03.018.

Bukovinszky, T., Helmsing, N.R., Grau, R.A., Bakker, E.S., Vos, M., Uittenhout, H., Verschoor, A.M., 2013. A device to study the behavioral responses of zooplankton to food quality and quantity. J. Insect Behav. 26, 453–465. https://doi.org/10.1007/s10905-012-9366-0.

Burns, A.L., Schaerf, T.M., Lizier, J., Kawaguchi, S., Cox, M., King, R., Krause, J., Ward, A.J.W., 2022. Self-organization and information transfer in Antarctic krill swarms. Proc. R. Soc. B Biol. Sci. 289 (1969), 20212361. https://doi.org/10.1098/rspb.2021.2361.

Buskey, E.J., Peterson, J.O., Ambler, J.W., 1995. The role of photoreception in the swarming behavior of the copepod *Dioithona oculata*. Mar. Freshw. Behav. Physiol. 26 (2–4), 273–285. https://doi.org/10.1080/10236249509378946.

Calovi, D.S., Litchinko, A., Lecheval, V., Lopez, U., Pérez Escudero, A., Chaté, H., Sire, C., Theraulaz, G., 2018. Disentangling and modeling interactions in fish with burst-and-coast swimming reveal distinct alignment and attraction behaviors. PLoS Comput. Biol. 14 (1), e1005933. https://doi.org/10.1371/journal.pcbi.1005933.

Cavagna, A., Giardina, I., 2014. Bird flocks as condensed matter. Annu. Rev. Condens. Matter Phys. 5 (1), 183–207. https://doi.org/10.1146/annurev-conmatphys-031113-133834.

Clutter, R.I., 1969. The microdistribution and social behavior of some pelagic mysid shrimps. J. Exp. Mar. Biol. Ecol. 3 (2), 125–155. https://doi.org/10.1016/0022-0981(69)90012-4.

Codling, E.A., Bode, N.W., 2014. Copycat dynamics in leaderless animal group navigation. Mov. Ecol. 2, 11. https://doi.org/10.1186/2051-3933-2-11.

Codling, E.A., Pitchford, J.W., Simpson, S.D., 2007. Group navigation and the "many-wrongs principle" in models of animal movement. Ecology 88 (7), 1864–1870. https://doi.org/10.1890/06-0854.1.

Colizzi, E.S., Vroomans, R.M., Merks, R.M., 2020. Evolution of multicellularity by collective integration of spatial information. eLife 9, e56349. https://doi.org/10.7554/eLife.56349.

Cottier, F.R., Tarling, G.A., Wold, A., Falk-Petersen, S., 2006. Unsynchronised and synchronised vertical migration of zooplankton in a high Arctic fjord. Limnol. Oceanogr. 51 (6), 2586–2599. https://doi.org/10.4319/lo.2006.51.6.2586.

Couzin, I.D., Krause, J., James, R., Ruxton, G.D., Franks, N.R., 2002. Collective memory and spatial sorting in animal groups. J. Theor. Biol. 218 (1), 1–11. https://doi.org/10.1006/jtbi.2002.3065.

Danielopol, D.L., Swanson, K.M., 2019. Ostracod phylogeny and evolution: thirty years after "Manawan perspective". Geo-Eco-Mar. 25, 219–251. https://doi.org/10.5281/zenodo.3607270.

Davidson, J.D., Sosna, M.M.G., Twomey, C.R., Sridhar, V.H., Leblanc, S.P., Couzin, I.D., 2021. Collective detection based on visual information in animal groups. J. R. Soc. Interface 18 (180), 20210142. https://doi.org/10.1098/rsif.2021.0142.

De, R., Chakraborty, D., 2022. Collective motion: influence of local behavioural interactions among individuals. J. Biosci. 47, 48. https://doi.org/10.1007/s12038-022-00277-4.

Dell, A.I., Bender, J.A., Branson, K., Couzin, I.D., de Polavieja, G.G., Noldus, L.P., Pérez-Escudero, A., Perona, P., Straw, A.D., Wikelski, M., Brose, U., 2014. Automated image-based tracking and its application in ecology. Trends Ecol. Evol. 29 (7), 417–428. https://doi.org/10.1016/j.tree.2014.05.004.

Dodson, S.I., Ryan, S., Tollrian, R., Lampert, W., 1997. Individual swimming behavior of *Daphnia*: effects of food, light and container size in four clones. J. Plankton Res. 19 (10), 1537–1552. https://doi.org/10.1093/plankt/19.10.1537.

Durieux, D., Fassotte, B., Deneubourg, J.-L., Brostaux, Y., Vandereycken, A., Joie, E., Haubruge, E., Verheggen, F.J., 2014. Aggregation behavior of *Harmonia axyridis* under non-wintering conditions. Insect Sci. 22 (5), 670–678. https://doi.org/10.1111/1744-7917.12144.

Dutta, A., Zisserman, A., 2019. The VIA annotation software for images, audio and video. In: Proceedings of the 27th ACM International Conference on Multimedia (MM '19), pp. 2276–2279. https://doi.org/10.1145/3343031.3350535.

Enright, J.T., Hamner, W.M., 1967. Vertical diurnal migration and endogenous rhythmicity. Science 157 (3791), 937–941. https://doi.org/10.1126/science.157.3791.937.

Flierl, G.R., Woods, N.W., 2015. Copepod aggregations: influences of physics and collective behavior. J. Stat. Phys. 158 (3), 665–698. https://doi.org/10.1007/s10955-014-1162-0.

Forward Jr., R.B., 1980. Phototaxis of a sand-beach amphipod: physiology and tidal rhythms. J. Comp. Physiol. 135, 243–250. https://doi.org/10.1007/BF00657252.

Frenzel, P., Boomer, I., 2005. The use of ostracods from marginal marine, brackish waters as bioindicators of modern and quaternary environmental change. Palaeogeogr. Palaeoclimatol. Palaeoecol. 225 (1–4), 68–92. https://doi.org/10.1016/j.palaeo.2004.02.051.

Galbiati, M., Lapadula, S., Forlani, M., Barzaghi, B., Manenti, R., 2023. Both light stimuli and predation risk affect the adult behavior of a stygobiont crustacean. Diversity 15 (2), 290. https://doi.org/10.3390/d15020290.

Gerhardt, A., de Bisthoven, L.J., Schmidt, S., 2006. Automated recording of vertical negative phototactic behaviour in *Daphnia magna* Straus (Crustacea). Hydrobiologia 559, 433–441. https://doi.org/10.1007/s10750-005-1259-1.

Gerrish, G.A., Morin, J.G., 2016. Living in sympatry via differentiation in time, space and display characters of courtship behaviors of bioluminescent marine ostracods. Mar. Biol. 163, 190. https://doi.org/10.1007/s00227-016-2960-5.

Graham, W.M., Pagès, F., Hamner, W.M., 2001. A physical context for gelatinous zooplankton aggregations: a review. Hydrobiologia 451, 199–212. https://doi.org/10.1023/A:1011876004427.

Hamilton, W.J., 1967. Social aspects of bird orientation mechanisms. In: Storm, R.M. (Ed.), Animal Orientation and Navigation. Oregon State University Press, Corvallis, OR, USA, pp. 57–59.

Hensley, N.M., Rivers, T.J., Gerrish, G.A., Saha, R., Oakley, T.H., 2023. Collective synchrony of mating signals modulated by ecological cues and social signals in bioluminescent sea fireflies. Proc. R. Soc. B Biol. Sci. 290, 20232311. https://doi.org/10.1098/rspb.2023.2311.

Herbert-Read, J.E., Krause, S., Morrell, L.J., Schaerf, T.M., Krause, J., Ward, A.J.W., 2013. The role of individuality in collective group movement. Proc. R. Soc. B Biol. Sci. 280 (1752), 20122564. https://doi.org/10.1098/rspb.2012.2564.

Horne, D.J., Cohen, A., Martens, K., 2002. Taxonomy, morphology and biology of quaternary and living Ostracoda. In: Holmes, J.A., Chivas, A.R. (Eds.), The Ostracoda: Applications in Quaternary Research. American Geophysical Union, pp. 5–36. https://doi.org/10.1029/131GM02.

Jeanson, R., Dussutour, A., Fourcassié, V., 2012. Key factors for the emergence of collective decision in invertebrates. Front. Neurosci. 6, 121. https://doi.org/10.3389/fnins.2012.00121.

Jékely, G., 2009. Evolution of phototaxis. Philos. Trans. R. Soc. B 364 (1531), 2795–2808. https://doi.org/10.1098/rstb.2009.0072.

Jensen, K., Larsson, P., 2002. Predator evasion in *Daphnia*: the adaptive value of aggregation associated with attack abatement. Oecologia 132, 461–467. https://doi.org/10.1007/s00442-002-0979-4.

Jensen, K.H., Jakobsen, P.J., Kleiven, O.T., 1998. Fish kairomone regulation of internal swarm structure in *Daphnia pulex* (Cladocera: Crustacea). Hydrobiologia 368, 123–127. https://doi.org/10.1023/A:1003233728870.

Jensen, K.H., Kleiven, O.T., Jakobsen, P.J., 1999. How important is light in the aggregation behaviour of *Daphnia pulex* (Cladocera: Crustacea)? Hydrobiologia 411, 13–18. https://doi.org/10.1023/A:1003871116379.

Kao, C.-C., Chen, J., Chen, G.-F., Soong, K., 2010. Variable swarming time of an intertidal midge (*Pontomyia oceana* Tokunaga, 1964) controlled by a circadian clock and temperature. Mar. Freshw. Behav. Physiol. 43 (1), 1–9. https://doi.org/10.1080/10236240903495320.

Kesling, R.V., 1951. The morphology of ostracod molt stages. University of Illinois Press. https://doi.org/10.5962/bhl.title.50392.

Kirk, J.T.O., 2010. Light and Photosynthesis in Aquatic Ecosystems, 3rd ed. Cambridge University Press, Cambridge. https://doi.org/10.1017/CBO9781139168212.

Klamser, P.P., Gómez-Nava, L., Landgraf, T., Jolles, J.W., Bierbach, D., Romanczuk, P., 2021. Impact of variable speed on collective movement of animal groups. Front. Phys. 9, 715996. https://doi.org/10.3389/fphy.2021.715996.

Klie, W., 1926. Ostracoda. In P. Schulze (Ed.), Biologie der Tiere Deutschlands (Teil 22, pp. 1–56). Gebrüder Borntraeger.

Leising, A.W., Yen, J., 1997. Spacing mechanisms within light-induced copepod swarms. Mar. Ecol. Prog. Ser. 155, 127–135. https://doi.org/10.3354/meps155127.

Macquart-Moulin, C., 1973. Le comportement d'essaim chez les Mysidacés: Influence de l'intensité lumineuse sur la formation, le maintien et la dissociation des essaims de *Leptomysis lingvura*. Rapp. Comm. Int. Mer Méditerr. 21, 499–501.

Mann, R.P., Bailey, J.D., Codling, E.A., 2024. Accuracy, rationality and specialization in a generalized model of collective navigation. J. R. Soc. Interface 21 (218), 20240207. https://doi.org/10.1098/rsif.2024.0207.

Meisch, C., 2000. Crustacea: Ostracoda. Freshwater Ostracoda of Western and Central Europe. Spektrum Akademischer Verlag, Heidelberg/Berlin. ISBN 3–8274–1001-0.

Michels, E., De Meester, L., 1998. The influence of food quality on the phototactic behaviour of *Daphnia magna* Straus. Hydrobiologia 379, 199–206. https://doi.org/10.1023/A:1003496000796.

Miličić, D., Savić, T., Petković, B., Potrebić, M., Trajković, J., Pavković-Lučić, S., 2019. Behavioural responses of the non-marine ostracod *Heterocypris incongruens* (Crustacea: Ostracoda) to natural chemical cues: Laboratory observations. In: Lachance, N. (Ed.), The Zoological Guide to Crustacea. Nova Science Publishers, New York, pp. 89–112 (ISBN 978-1-53616-366-7).

Miličić, D.M., Majstorović, A.P., Pavković-Lučić, S.B., Savić, T.T., 2015. Behaviour and food selection of *Heterocypris incongruens* (Ostracoda). Crustaceana 88 (10−11), 1097–1110. https://doi.org/10.1163/15685403-00003479.

Modlin, R.F., 1990. Observations on the aggregative behavior of *Mysidium columbiae*, the mangrove mysid. Mar. Ecol. 11 (3), 263–275. https://doi.org/10.1111/j.1439-0485.1990.tb00244.x.

Nuttall, P.M., Fernando, C.H., 1970. Notes on aggregation observed in two species of freshwater Ostracoda. Can. J. Zool. 48 (2), 392–393. https://doi.org/10.1139/z70-063.

O'Brien, D.P., 1988. Direct observations of clustering (schooling and swarming) behaviour in mysids (Crustacea: Mysidacea). Mar. Ecol. Prog. Ser. 42 (3), 235–246. https://doi.org/10.3354/meps042235.

Ohtsuka, S., Inagaki, H., Onbe, T., Gushima, K., Yoon, Y.H., 1995. Direct observations of groups of mysids in shallow coastal waters of western Japan and southern Korea. Mar. Ecol. Prog. Ser. 123, 33–44. https://doi.org/10.3354/meps123033.

Okubo, A., 1980. Diffusion and Ecological Problems: Mathematical Models. Biomathematics, vol. 10. Springer.

Ordemann, A., Balázsi, G., Moss, F., 2003. Pattern formation and stochastic motion of the zooplankton *Daphnia* in a light field. Phys. A Stat. Mech. Appl. 325 (1–2), 260–266. https://doi.org/10.1016/S0378-4371(03)00204-8.

Ottonello, D., Romano, A., 2011. Ostracoda and Amphibia in temporary ponds: who is the prey? Unexpected trophic relation in a Mediterranean freshwater habitat. Aquat. Ecol. 45, 55–62. https://doi.org/10.1007/s10452-010-9323-y.

Pijanowska, J., Kowalczewski, A., 1997. Predators can induce swarming behaviour and locomotory responses in *Daphnia*. Freshw. Biol. 37 (3), 649–656. https://doi.org/10.1046/j.1365-2427.1997.00192.x.

Rajewicz, W., Romano, D., Schmickl, T., Thenius, R., 2023. *Daphnia*'s phototaxis as an indicator in ecotoxicological studies: a review. Aquat. Toxicol. 265, 106762. https://doi.org/10.1016/j.aquatox.2023.106762.

Ringelberg, J., 1995. Changes in light intensity and diel vertical migration: a comparison of marine and freshwater environments. J. Mar. Biol. Assoc. U. K. 75 (1), 15–25. https://doi.org/10.1017/S0025315400015162.

Rivers, T.J., Morin, J.G., 2008. Complex sexual courtship displays by luminescent male marine ostracods. J. Exp. Biol. 211 (14), 2252–2262. https://doi.org/10.1242/jeb.011130.

Robert, M., Dagorn, L., Lopez, J., Moreno, G., Deneubourg, J.-L., 2013. Does social behavior influence the dynamics of aggregations formed by tropical tunas around floating objects? An experimental approach. J. Exp. Mar. Biol. Ecol. 440, 238–243. https://doi.org/10.1016/j.jembe.2013.01.005.

Romano, D., Rossetti, G., Stefanini, C., 2022. Learning on a chip: towards the development of trainable biohybrid sensors by investigating cognitive processes in non-marine Ostracoda via a miniaturised analytical system. Biosyst. Eng. 213, 162–174. https://doi.org/10.1016/j.biosystemseng.2021.11.004.

Rossi, V., Benassi, G., Belletti, F., Menozzi, P., 2011. Colonization, population dynamics, predatory behaviour and cannibalism in *Heterocypris incongruens* (Crustacea: Ostracoda). J. Limnol. 70, 102–108. https://doi.org/10.4081/jlimnol.2011.102.

Sasaki, T., Masuda, N., Mann, R.P., Biro, D., 2022. Empirical test of the many-wrongs hypothesis reveals weighted averaging of individual routes in pigeon flocks. iScience 25 (10), 105076. https://doi.org/10.1016/j.isci.2022.105076.

Shen, A., Zhou, F., Jia, Y., Wang, R., Liu, C., Duan, C., MacIsaac, H.J., Lauridsen, T.L., Pan, Y., 2025. Altered underwater light characteristics impact photoreceptive mesozooplankton and macrozooplankton from physiological responses to community dynamics. Ecol. Indic. 178, 114011. https://doi.org/10.1016/j.ecolind.2025.114011.

Simons, A.M., 2004. Many wrongs: the advantage of group navigation. Trends Ecol. Evol. 19 (9), 453–455. https://doi.org/10.1016/j.tree.2004.07.001.

Sohn, I.G., Kornicker, L.S., 1972. Predation of schistosomiasis vector snails by Ostracoda (Crustacea). Science 175 (4027), 1258–1259. https://doi.org/10.1126/science.175.4027.1258.

Stearns, D.E., Forward Jr., R.B., 1984. Copepod photobehavior in a simulated natural light environment and its relation to nocturnal vertical migration. Mar. Biol. 82, 91–100. https://doi.org/10.1007/BF00392767.

Storz, U.C., Paul, R.J., 1998. Phototaxis in water fleas (*Daphnia magna*) is differently influenced by visible and UV light. J. Comp. Physiol. A. 183, 709–717. https://doi.org/10.1007/s003590050293.

Sumpter, D.J.T., Pratt, S.C., 2009. Quorum responses and consensus decision making. Philos. Trans. R. Soc. B 364, 743–753. https://doi.org/10.1098/rstb.2008.0204.

Suriyampola, P.S., Iruri-Tucker, A.A., Padilla-Veléz, L., Enriquez, A., Shelton, D.S., Martins, E.P., 2022. Small increases in group size improve small shoals' response to water flow in zebrafish. J. Zool. 316 (4), 271–281. https://doi.org/10.1111/jzo.12952.

Tao, Z., Wang, Y., Wang, J., Liu, M., Zhang, W., 2019. Photobehaviors of the calanoid copepod *Calanus sinicus* from the Yellow Sea to visible and UV-B radiation as a function of wavelength and intensity. J. Oceanol. Limnol. 37 (4), 1289–1300. https://doi.org/10.1007/s00343-019-8163-4.

Van Gool, E., Ringelberg, J., 2002. Relationship between fish kairomone concentration in a lake and phototactic swimming by *Daphnia*. J. Plankton Res. 24 (7), 713–721. https://doi.org/10.1093/plankt/24.7.713.

Vicsek, T., Zafeiris, A., 2012. Collective motion. Phys. Rep. 517 (3–4), 71–140. https://doi.org/10.1016/j.physrep.2012.03.004.

Wallraff, H.G., 1978. Social interrelations involved in migratory orientation of birds: possible contribution of field studies. Oikos 30, 401–404. https://doi.org/10.2307/3543490.

Wiese, K., 1996. Sensory capacities of euphausiids in the context of schooling. Mar. Freshw. Behav. Physiol. 28 (3), 183–194. https://doi.org/10.1080/10236249609378989.

Yu, J.H., Napoli, J.L., Lovett-Barron, M., 2024. Understanding collective behavior through neurobiology. Curr. Opin. Neurobiol. 86, 102866. https://doi.org/10.1016/j.conb.2024.102866.

Zhang, J., Yasuhara, M., Wei, C.-L., Tian, S.Y., Aye, K.K.T., Gemery, L., Cronin, T.M., Frenzel, P., Horne, D.J., 2024. Sight and blindness: the relationship between ostracod eyes, water depth, and light availability in the Arctic Ocean. Limnol. Oceanogr. 69 (6), 1418–1428. https://doi.org/10.1002/lno.12584.